Article

# Synthesis of Colloidal Pd/Au Dilute Alloy Nanocrystals and Their Potential for Selective Catalytic Oxidations

Cody J. Wrasman, Alexey Boubnov, Andrew R. Riscoe, Adam S. Hoffman, Simon R. Bare, and Matteo Cargnello

*J. Am. Chem. Soc.*, **Just Accepted Manuscript** • DOI: 10.1021/jacs.8b07515 • Publication Date (Web): 17 Sep 2018

# Synthesis of Colloidal Pd/Au Dilute Alloy Nanocrystals and Their Potential for Selective Catalytic Oxidations

Cody J. Wrasman[1], Alexey Boubnov[2], Andrew R. Riscoe[1], Adam S. Hoffman[2], Simon R. Bare[2], Matteo Cargnello[1,*]

[1]*Department of Chemical Engineering and SUNCAT Center for Interface Science and Catalysis, Stanford University, Stanford, California, 94305, United States.*

[2]*SLAC National Accelerator Laboratory, Menlo Park, California, 94025, United States*

Keywords: palladium, gold, dilute alloys, nanocrystals, oxidation

## ABSTRACT

Selective oxidations are crucial for the creation of valuable chemical building blocks but often require expensive and unstable stoichiometric oxidants such as hydroperoxides and peracids. To date, many catalysts that contain a single type of active site have not been able to attain the desired level of selectivity for partially oxidized products over total combustion. However, catalysts containing multiple types of active sites have proven to be successful for selective reactions. One category of such catalysts is bimetallic alloys, in which catalytic activity and selectivity can be tuned by modifying the surface composition. Traditional catalyst synthesis methods using impregnation struggle to create catalysts with sufficient control over surface chemistry to accurately tune the ensemble size of desired active sites. Here we describe the synthesis of colloidal nanocrystals of dilute alloys of palladium and gold. We show that when supported on titania ($TiO_2$), tuning the composition of the Pd/Au nanocrystal surface provides a synergistic effect in the selective oxidation of 2-propanol to acetone in the presence of $H_2$ and $O_2$. In particular, we show that certain Pd/Au surface ratios exhibit activity and selectivity far superior to Pd or Au individually. Through precise structural characterization we demonstrate that isolated atoms of Pd exist in the most active catalysts. The synergy between isolated Pd atoms and Au allows for the formation of reactive oxidizing species, likely hydroperoxide groups, responsible for selective oxidation while limiting oxygen dissociation and thus, complete combustion. This work opens the way to more efficient utilization of scarce noble metals and new options for catalyzed selective oxidations.

## INTRODUCTION

Selective oxidations are essential for adding functionality to molecules to make desired products and enable future chemical modification. However, most of these reactions require the use of expensive or corrosive oxidants due to the lack of selectivity of molecular oxygen as an oxidant, especially on platinum group metals. Over three decades ago, small Au nanocrystals were found to catalyze oxidation reactions.[1] Since then, Au has been shown to be active for epoxidation reactions,[2–4] carbon monoxide oxidation,[1,5] and selective hydrocarbon oxidation,[6,7] all using molecular oxygen. Au is advantageous for selective oxidation reactions compared to more traditional oxidation catalysts like Pd or Pt because of its weak oxygen dissociative chemisorption ability, which leads to selective rather than complete oxidation. Selective oxidation activity on Au is further enhanced under hydro-oxidation conditions which include a hydrogen co-feed.[8] Stemming from work in propylene epoxidation,[2] it has been found that co-feeding $O_2$ and $H_2$ over catalysts composed of Au on Ti-containing supports generates hydroperoxide intermediates,[6–9] and gas phase hydrogen peroxide.[10] These intermediates have been observed by several spectroscopic techniques.[7,9,11,12] It has been hypothesized that during propylene epoxidation, Au nanoparticles stabilize molecular oxygen, which then reacts with activated H atoms to form either adsorbed OOH or $H_2O_2$. These hydroperoxide species diffuse to Ti(IV) sites on the support near the Au nanocrystals where the oxidation reaction occurs.[6,7,9] Despite the improvement in the performance when hydro-oxidation conditions are used, reaction rates are still low because it is hypothesized that the reaction is limited by the rate of dissociative chemisorption of $H_2$ at the Au-support interface with the assistance of adsorbed $O_2$.[13,14]

Dilute, or single atom alloy (SAA) catalysts, where isolated atoms of one metal are added to a host metal,[15] have been shown to be adept at dissociative chemisorption of $H_2$.[15–20] In most

cases single atoms of a platinum group metal are alloyed with a coinage metal. In this dilute alloy, the probability of having two or more contiguous platinum group metal atoms present on the surface of the nanoparticle is extremely low, thus eliminating the possibility of finding bridge and three-fold binding sites of the platinum group metal. As a result, the binding modes of the chemisorbed species on the platinum group metal change due to the elimination of the stronger binding sites between its atoms. In this way, SAAs provide pathways to increased selectivity and poison resistance that is unattainable in the bulk metal.[21] It has been found that the isolated platinum group metal atoms are capable of dissociative $H_2$ chemisorption, which then spills over onto the coinage metal surface.[17,18] For example, Sykes and coworkers showed that single atoms of Pd dispersed on a Au surface were capable of carrying out $H_2/D_2$ scrambling to form HD, whereas pure Au surfaces were completely inactive.[18] The coinage metals can then utilize the spilled over hydrogen atoms to carry out highly selective hydrogenation reactions.[15,16,19,20]

There are no reports of SAA catalysts used for partial oxidation reactions, partially due to the required ensemble sizes for oxygen activation.[22,23] For example, Goodman and coworkers found that two adjacent Pd atoms, a motif not present in SAAs, are required to dissociate oxygen, a common step in oxidation reactions, in Pd/Au alloys.[22] However, our hypothesis is that the inability of isolated platinum group atom geometries to chemisorb oxygen dissociatively combined with the high hydrogen activation performance of SAAs can be leveraged to produce enhanced hydro-oxidation catalysis. Thus, while Au/oxide interfaces are still present for the formation of hydroperoxy intermediates, isolated atoms of platinum group metals would assist in the rate limiting step of dissociating hydrogen. A SAA catalyst may therefore be able to increase the rate of production of reactive oxidizing species and increase the overall rate of selective oxidation while maintaining the selectivity of Au catalysts.

In order to take advantage of the benefits of single atom geometries and to avoid the formation of byproducts on unselective phases, control over the structure and morphology of supported catalysts is crucial. The presence of impurity phases that contain extended surfaces of a platinum group metal could reduce the selectivity of the oxidation process, and complicate the understanding of reaction mechanisms and structure-property relationships. In this work we detail the synthesis and characterization of dilute Pd on Au alloy nanocrystals with high control and uniformity as well as their utilization in the selective oxidation of 2-propanol to acetone, a reaction studied previously on pure Au.[24–27] Specifically, we compare the catalytic activity on pure Au and Pd individually to that of Pd/Au SAA nanocrystals under oxidizing and hydro-oxidizing conditions. We find that Au nanocrystal surfaces containing single atoms of Pd are more active and selective than either of the pure metals under hydro-oxidation conditions. These results highlight the selectivity attainable with SAAs catalysts and create new possibilities for the use of SAAs as oxidation catalysts.

## EXPERIMENTAL SECTION

**Synthesis of Au Nanocrystals (NCs).** Au NCs were synthesized using previously reported procedures with slight modification.[28] A reducing solution was first prepared by dissolving borane tert-butylammine complex (TBAB 88.6 mg, 97%, Aldrich) in a mixture of oleylamine (OLAM, 2 mL, 70%, Aldrich) and tetralin (1,2,3,4 tetrahydronaphthalene, 2 mL, 98%, Acros) with sonication. $HAuCl_4 \cdot 3H_2O$ (200 mg, ACS Reagent Grade, Acros) was dissolved in OLAM (20 mL) and tetralin (20 mL) using magnetic stirring at 40 °C to form an orange solution. Immediately after the $HAuCl_4 \cdot 3H_2O$ was dissolved the reducing solution was injected

instantaneously, causing an immediate color change to dark purple. The mixture was allowed to stir for 1 h before particles were recovered by precipitation using isopropanol (5 mL) and ethanol (25 mL) followed by centrifugation (8000 rpm, 3 min). The particles were redissolved in hexanes (Certified ACS, Fisher) and the precipitation process was repeated twice more. The clear supernatant was discarded and the particles were redispersed in 10 mL of hexanes. The above synthesis yielded uniform NCs with an average diameter of 2.8 ± 0.4 nm. The average Au NC size can be tuned by modifying the synthesis temperatures as described by Peng and coworkers with lower temperatures yielding larger NCs.[28] NCs with a diameter of 2.8 ± 0.4, 3.8 ± 0.4 , and 5.5 ± 0.5 nm were obtained by using a reaction temperatures of 40 °C, 32 °C, and 8 °C respectively.

**Synthesis of Pd NCs.** Pd NCs were synthesized using previously reported procedures[29] targeting a final diameter of 4 nm. Palladium acetylacetonate (307.9 mg, 35%, Acros) was dissolved in a mixture of octadecene (ODE, 21 mL, 90%, Acros) and tetradecene (TDE, 19 mL, 94%, Alfa Aesar). OLAM (0.84 mL) and oleic acid (OLAC, 1.6 mL, 90%, Aldrich) were added and the mixture was degassed (pressure <2 mTorr) for 30 minutes. Trioctylphosphine (1.16 mL, 97% Aldrich) was then injected under vacuum and the mixture was heated to 50 °C and held there for 30 minutes. The mixture was then placed under static nitrogen and heated at 25 $^{o}$C min$^{-1}$ to 280 °C. At this temperature the mixture of octadecene and tetradecene began to reflux. After 15 minutes of reflux, the mixture was cooled to room temperature. The NCs were precipitated with ethanol (20 mL) and isopropanol (5 mL) and recovered by centrifugation (8000 rpm, 3 min) three times, redispersing with hexanes and 10 μL oleylamine in between each round of precipitation. The final NCs had an average size of 2.8 ± 0.3 nm and were dispersed in hexanes.

**Synthesis of Pd/Au NCs.** Pd/Au NCs were synthesized using a modified seed mediated

process.[30] Au NCs (30 mg) in hexanes, OLAM (30 mL), OLAC (1.9 mL), and $Pd(NO_3)_2 \cdot 3H_2O$ (40% Pd, Aldrich) were mixed in a three neck flask with magnetic stirring and degassed at 50 °C for 30 minutes. For the low Pd content sample 2.8 mg $Pd(NO_3)_2 \cdot 3H_2O$ were used while for the high Pd content sample 17.6 mg $Pd(NO_3)_2 \cdot 3H_2O$ were used. The mixture was then put under flowing nitrogen, heated to 140 °C, and stirred for 30 minutes. Mixtures were then cooled to room temperature and the Pd/Au NCs were recovered by precipitating in isopropanol (5 mL) and ethanol (25 mL) and centrifugation (8000 rpm, 3 min) three times, redissolving in hexanes in between each precipitation. Finally the particles were dissolved in hexanes (5 mL). The Pd/Au NC synthesis can be used to control the amount of Pd added to the Au seeds with larger amounts of $Pd(NO_3)_2 \cdot 3H_2O$ resulting in greater Pd content in the final NCs.

**Catalyst Preparation.** NCs were loaded onto P25 $TiO_2$ (Aeroxide, Acros, previously calcined in air at 500 °C for 5 hours) by first dispersing the $TiO_2$ powder in a flask in hexanes with vigorous stirring. A solution of NCs in hexanes was then added to the flask to give a nominal total final metal loading of 0.5 wt. % (ICP-MS was used to confirm the final metal loading). In a typical procedure, 1.75 g $TiO_2$ was dispersed by sonication in 25 mL hexanes and added to 1.9 mL of 4.6 mg $mL^{-1}$ Pd/Au NC in hexanes solution. The mixture was stirred for 5 minutes and the solids were recovered via centrifugation (8000 rpm for 3 min). The clear supernatant was discarded and the solid was dried at room temperature overnight. The powder was then ground and sieved through a 180 mesh sieve. NC ligands were removed by a rapid heat treatment,[31] where the powders were inserted into a furnace preheated to 700 °C for 30 seconds in air.

**Catalyst Characterization.** Transmission electron microscopy (TEM) images were collected on a FEI Tecnai transmission electron microscope equipped with an Orius CCD operating at 200 kV. NC solutions were drop-cast onto ultrathin carbon films supported on Cu (Electron

Microscopy Sciences) while supported NC catalysts were dispersed in 2-propanol prior to drop-casting onto lacy-carbon films supported on Cu (Electron Microscopy Science). Particle size distributions were calculated using ImageJ software with at least 100 particles per sample. NC solutions were analyzed using a Cary 300 UV-Vis spectrophotometer by first diluting 20 μL in 3 mL hexanes. Spectra were collected between wavelengths of 200 and 800 nm.

X-ray absorption spectra were recorded at the Stanford Synchrotron Radiation Lightsource (SSRL, California, USA) at wiggler beam lines 7-3 and 4-1 for the Pd K-edge (24350 eV) and Au $L_3$-edge (11919 eV), respectively, each using a Si(220) double-crystal monochromator. The storage ring was operated at 3 GeV with a ring current of 494-500 mA in top-up mode. Pd K-edge data were recorded in fluorescence mode, using a 32-element liquid nitrogen-cooled Ge detector (Canberra) and Au $L_3$-edge data was acquired in transmission mode. The Pd/Au/$TiO_2$ catalysts were investigated after ligand removal as self-supporting pellets with an appropriate absorption length to prevent self-absorption at the Pd edge.

The raw data were processed using the Athena interface of the Demeter software package.[32] The spectra were energy-calibrated, merged and normalized. The extended X-ray absorption fine structure (EXAFS) was extracted in k-space and Fourier-transformation was conducted on the $k^3$-weighted EXAFS function ($k$ = 3.0–11.5 $Å^{-1}$) to amplify the oscillations at high $k$-values. Phase shifts and amplitudes for relevant back-scattering paths were calculated using FEFF6 from crystallographic information files (CIF) of PdO (ICSD code 36598), Pd metal (ICSD code 76148), Au metal (ICSD code 44362), and Au3Pd fcc-alloy (ICSD code 180873). EXAFS modeling was carried out on an R-range of 1.3-3.3 Å taking into account $k_1$, $k_2$, and $k_3$-weighting using the Artemis interface of the Demeter software.[32] $S_0^2$ was determined to be 0.78 ± 0.04 for the Pd K-edge from fitting Pd foil and 0.78 ± 0.05 for the Au $L_3$-edge from fitting Au

foil. According to the Nyquist criterion, a maximum of 11 parameters can be extracted from the EXAFS data in these ranges respectively. Pd K-edge EXAFS spectra were fitted with three nearest-neighbor shells: Pd-O from PdO (d = 2.01 Å, bulk CN = 4), Pd-Pd from Pd metal (d = 2.75 Å, bulk CN = 12) and Pd-Au from Au3Pd (d = 2.89 Å, bulk CN = 12). Au L3-edge EXAFS spectra were fitted using the Au-Pd and Au-Au shells from Au3Pd (d = 2.89 Å, bulk CN = 4) and Au-Au (d=2.89, bulk CN = 12) respectively. The EXAFS data from all the Pd/Au catalysts were modeled simultaneously to minimize errors.

Coordination numbers determined by EXAFS fitting were tested against coordination numbers predicted by two models based on surface alloying and bulk alloying. The surface-alloy model predicted Pd-Pd and Pd-Au coordination numbers, assuming that all Pd atoms were confined to the outer (111)-surface monolayer of the NC. Under this assumption, the surface concentration of Pd atoms was determined by the total Pd loading $x_{Pd}$ divided by the dispersion $D$ of the NC (fraction of surface atoms to total atoms), calculated from the mean particle diameter $\langle d \rangle$ using lattice parameters of Au by the relation.[33]

$$D = \frac{0.96\ \text{Å}}{\langle d \rangle}.$$

Pd-Pd coordination numbers were calculated within a slab of 7 atoms: 1 Pd absorber at center surrounded by 6 nearest neighbors (Pd or Au). Three sub-surface Au nearest neighbors were located under this slab. That implied a total $CN_{Pd\text{-}Pd} + CN_{Pd\text{-}Au} = 9$ with $CN_{Pd\text{-}Pd}$ ranging from 0 to 6 and $CN_{Pd\text{-}Au}$ ranging from 9 to 3 for near-zero to full Pd coverage.

Counts of 2 to 7 Pd atoms within the slab of 7 corresponded to Pd-Pd coordination numbers of 1 to 6. Using the binomial probability distribution of finding a given number of Pd

atoms as a function of the Pd surface concentration loading $x_{Pd}/D$, predicted coordination numbers were calculated using

$$\mathrm{CN}_{\text{Pd-Pd}} = \sum_{l=2}^{7} \sum_{k=l}^{7} \binom{7}{k} \left(\frac{x_{\mathrm{Pd}}}{D}\right)^{k} \left(1 - \frac{x_{\mathrm{Pd}}}{D}\right)^{7-k}.$$

This means adding up the counts of Pd atoms that correspond to each of the coordination numbers, each count multiplied by the probability that at least that number of sites is occupied by Pd.

The bulk-alloy model predicted a random mixture of Pd and Au in a bulk *fcc*-lattice, independent of the particle size. Based on 13-atom clusters of either 1 central Pd and 12 Pd/Au neighbors or 1 central Au and 12 Pd/Au neighbors, coordination numbers as a function of $x_{Pd}$ were calculated using the binomial distribution as

$$\mathrm{CN}_{\text{Pd-Pd}} = \sum_{l=2}^{13} \sum_{k=l}^{13} \binom{13}{k} x_{\mathrm{Pd}}^{k} (1 - x_{\mathrm{Pd}})^{13-k} \quad \text{and} \quad \mathrm{CN}_{\text{Au-Pd}} = \sum_{l=1}^{12} \sum_{k=l}^{13} \binom{13}{k} x_{\mathrm{Pd}}^{k} (1 - x_{\mathrm{Pd}})^{13-k}$$

respectively. The Pd-Pd and Pd-Au coordination numbers as well as Au-Pd and Au-Au summed to 12.

**Catalytic Measurements.** All catalytic measurements were collected at atmospheric pressure in a quartz U-tube reactor with an internal diameter of 1 cm. Supported catalysts (50 mg) were first physically mixed with calcined $TiO_2$ as a diluent (50 mg) to avoid reactor hot spots. The mixture was then loaded in between layers of acid washed quartz resulting in a bed length of 1 cm. The U-tube was heated using a Micromeritics furnace and the temperature was measured using a K-type thermocouple inserted inside the catalyst bed.

Reaction mixtures were prepared by feeding 5 vol. % $H_2$ in Ar (standard mixture, Airgas), 5 vol. % $O_2$ in Ar (standard mixture, Airgas), and Ar (99.999%, Airgas) through Brooks SLA5850 mass flow controllers. 2-propanol was added by feeding a separate Ar stream through a saturator filled with liquid 2-propanol at room temperature. Products were measured using a Buck Scientific Model 910 gas chromatograph equipped with a 6 ft Hayesep D column, a thermal conductivity detector, and a flame ionization detector with Ar as a carrier gas. Chromatograph peaks were deconvoluted using the Fityk software with Gaussian peak shapes.

Before starting reaction measurements, all catalysts were pretreated in a stream of 5 vol. % $O_2$ in Ar at 25 mL $min^{-1}$ for 60 minutes at 300 °C. The samples were then cooled to room temperature in Ar prior to introducing the reactant mixture.

## RESULTS AND DISCUSSION

We synthesized colloidal nanocrystals (NC) of dilute Pd/Au alloys following a Au seed mediated process modified from the literature.[30] The overall process is visualized in Scheme 1. We used the procedure of Sun and co-workers to synthesize Au NC seeds of different sizes.[28] The seeds were then introduced into a second colloidal synthesis along with different amounts of $Pd(NO_3)_2$ and heated to yield Pd/Au alloy NC with tunable Pd contents. This procedure for adding Pd works for all Au seed sizes and can therefore be used to make a variety of Pd/Au NC materials. There is a correspondence between the amount of $Pd(NO_3)_2$ included in the synthesis and the fraction of Pd in the final NC as determined by ICP-MS (Supporting Information Table S1). Through this procedure, independent control over particle size and surface composition is possible where conventional impregnation methods would result in separate phases of Au, Pd,

and Pd/Au alloy with different concentrations.

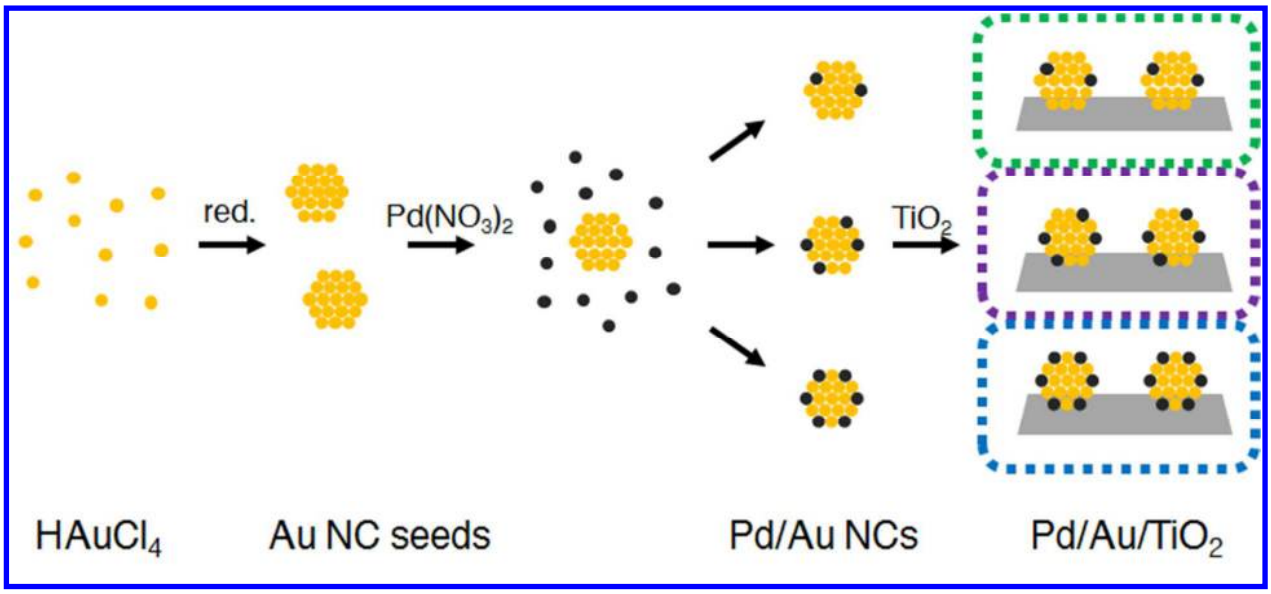


**Scheme 1.** Process flow of the Pd/Au on $TiO_2$ catalyst synthesis process. Au NCs are first colloidally synthesized with the final particle size determined by the synthesis temperature. After purification, the Au NCs of a given size are added to a second colloidal synthesis with the Pd precursor to create Pd/Au NCs. The amount of Pd in the second synthesis step determines the amount of Pd in the final catalyst. All Pd/Au NC in addition to pure Au and pure Pd NCs were then deposited onto calcined $TiO_2$ at 0.5 wt. % total metal loading.

Figure 1 (a-i) shows representative TEM images of the library of nine samples made with three different Au seed sizes (2.8 ± 0.4 nm, 3.8 ± 0.4 nm, and 5.5 ± 0.5 nm) each with three different concentrations of Pd, low (1.4-1.8% Pd), intermediate (4.1-6.9% Pd) and high (7.0-18.7% Pd). Particle size distributions of the nine NC samples demonstrate that all samples are uniform with narrow particle size distributions (Figure 1j). In particular, the absence of a

bimodal size distribution for Pd/Au NCs suggests that all of the Pd that was reduced out of solution was added to the Au seeds rather than forming separate Pd NCs. This conclusion is supported by UV-Vis spectroscopy characterization (Figure 2) which shows that the Au localized surface plasmon resonance (LSPR) peak was attenuated, but not eliminated, by the addition of Pd. The Au LSPR is indicative of Au domains and is strongly present in pure Au NCs.[28] Therefore, the inclusion of Pd in the Au domain is expected to cause a dampening of the Au LSPR, as is observed in the dilute Pd/Au alloy NCs.

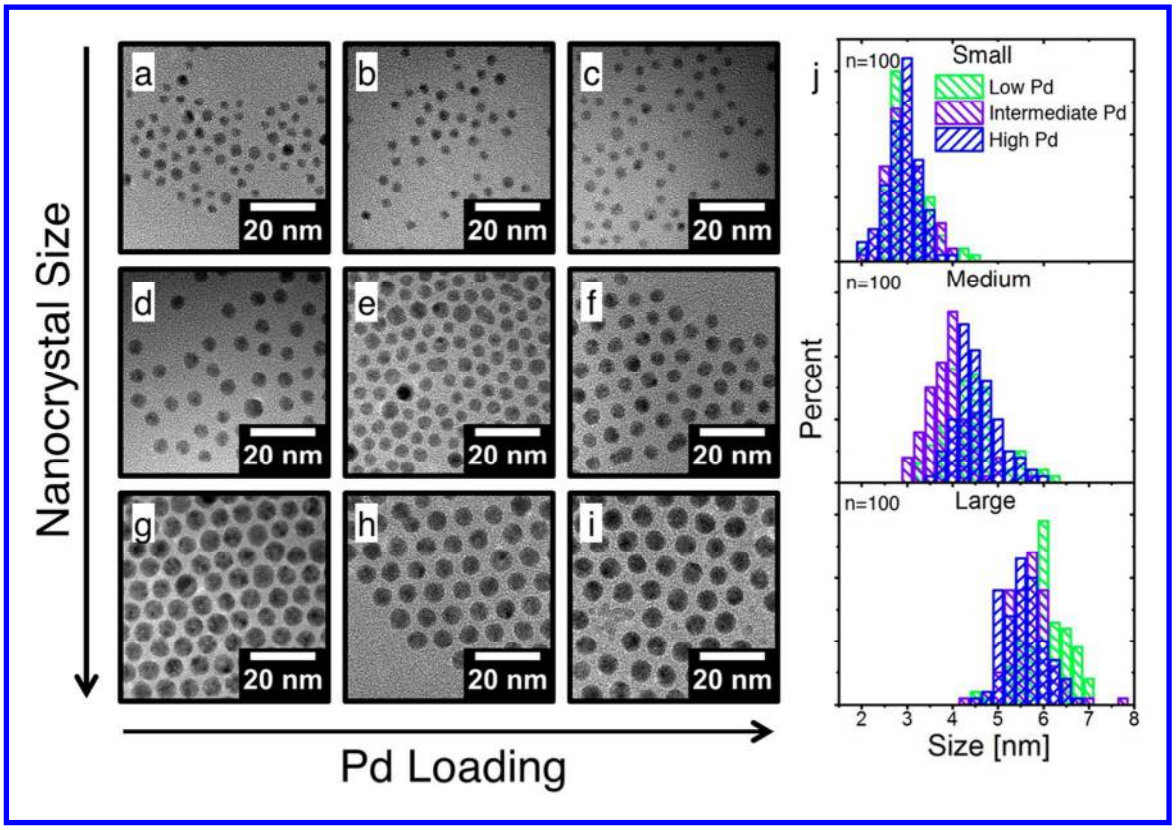


**Figure 1.** (a-i) TEM images of the library of nine Pd/Au catalysts arranged by Au NC seed size and Pd loading. (a-c): 2.8 ± 0.4 nm Au seeds; (d-f): 3.8 ± 0.4 nm Au seeds; (g-i): 5.5 ± 0.5 nm

Au seeds. (a, d, g): low Pd content; (b, e, h): intermediate Pd content; (c, f, i): high Pd content. (j) Particle size distributions of NCs corresponding to a specific Au seed size.

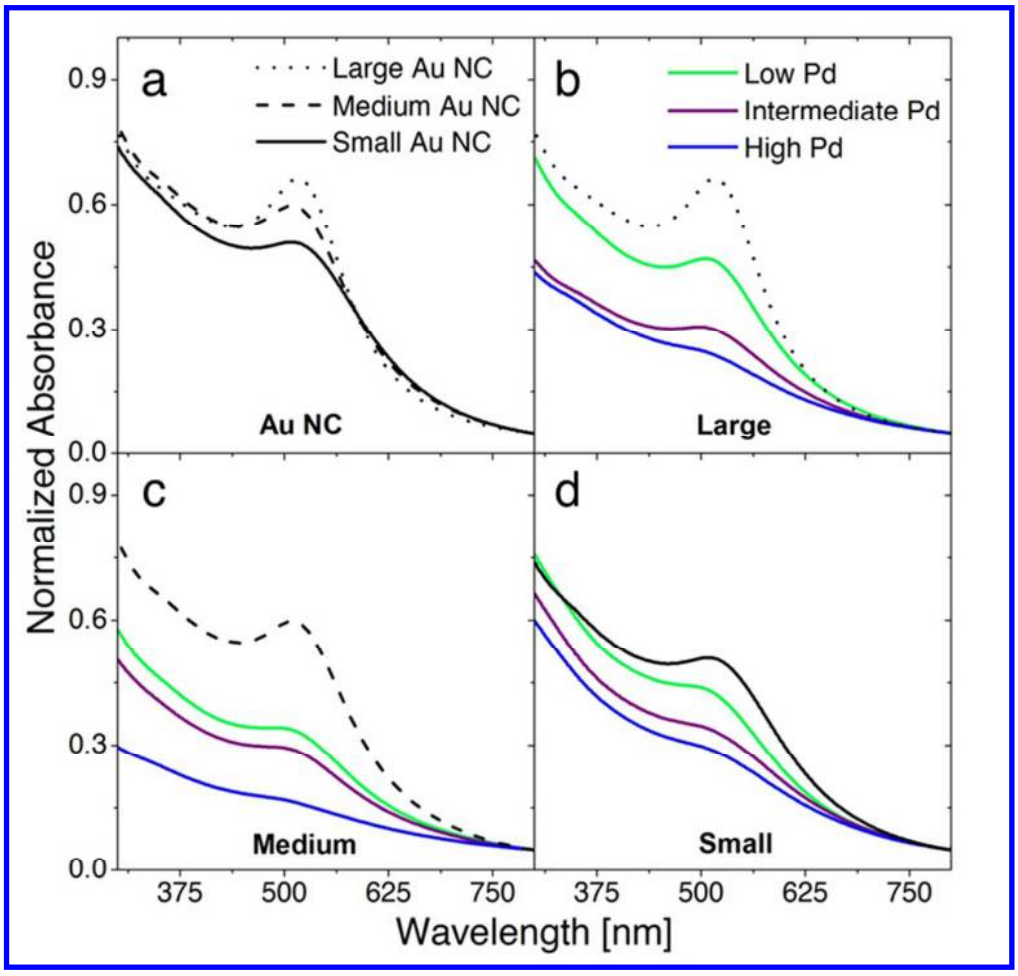


**Figure 2.** Normalized UV-Vis spectra for (a) all Au seed sizes (b) 5.5 nm seed Pd/Au NC (large), (c) 3.8 nm seed Pd/Au NC (medium), and (d) 2.8 nm seed Pd/Au NC (small).

The purified Pd/Au NC were then deposited onto calcined commercial $TiO_2$ (P25) that had been calcined at 500 °C for 5 hours in air to give a nominal total metal weight loading of 0.5 wt. %. The ligands on the NC surface were removed by a rapid thermal treatment, where the

supported samples were inserted into a furnace at 700 °C for 30 seconds.[31] Representative TEM images of the titania supported samples show minimal or no change in the particle size following deposition and ligand removal (Figure 3a) as well as after catalytic studies (Figure 3b, c).

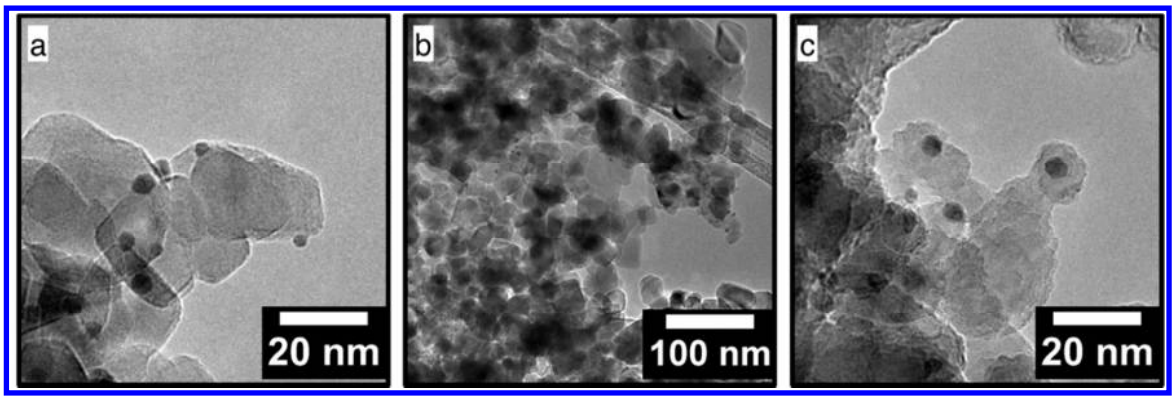


**Figure 3.** TEM of supported 3.3 nm Pd (4.8%)/Au NC (a) before and (b, c) after catalysis.

The Pd/Au/$TiO_2$ samples were characterized using X-ray absorption spectroscopy (XAS) to determine the average local geometric and electronic environment of each element. Figure 4 presents the extended X-ray absorption fine structure (EXAFS) and X-ray absorption near-edge structure (XANES) spectra and analysis at both the Pd K-edge and the Au $L_3$-edge for Pd/Au/$TiO_2$ catalysts made with the 2.8 ± 0.4 nm Au seeds. This series includes three levels of Pd, now referred to as Pd(1.4%)/Au, Pd(4.1%)/Au, and Pd(7.0%)/Au with increasing Pd concentration. The spectra and best fit models for the remaining six samples are presented in the supporting information in Figures S1 to S3, with the collected data of the best-fit model reported in Table S2. XANES spectra and the EXAFS spectra with best-fit models for the three supported alloys are shown in Figure 4 and are reported for both Pd and Au in Table 1.

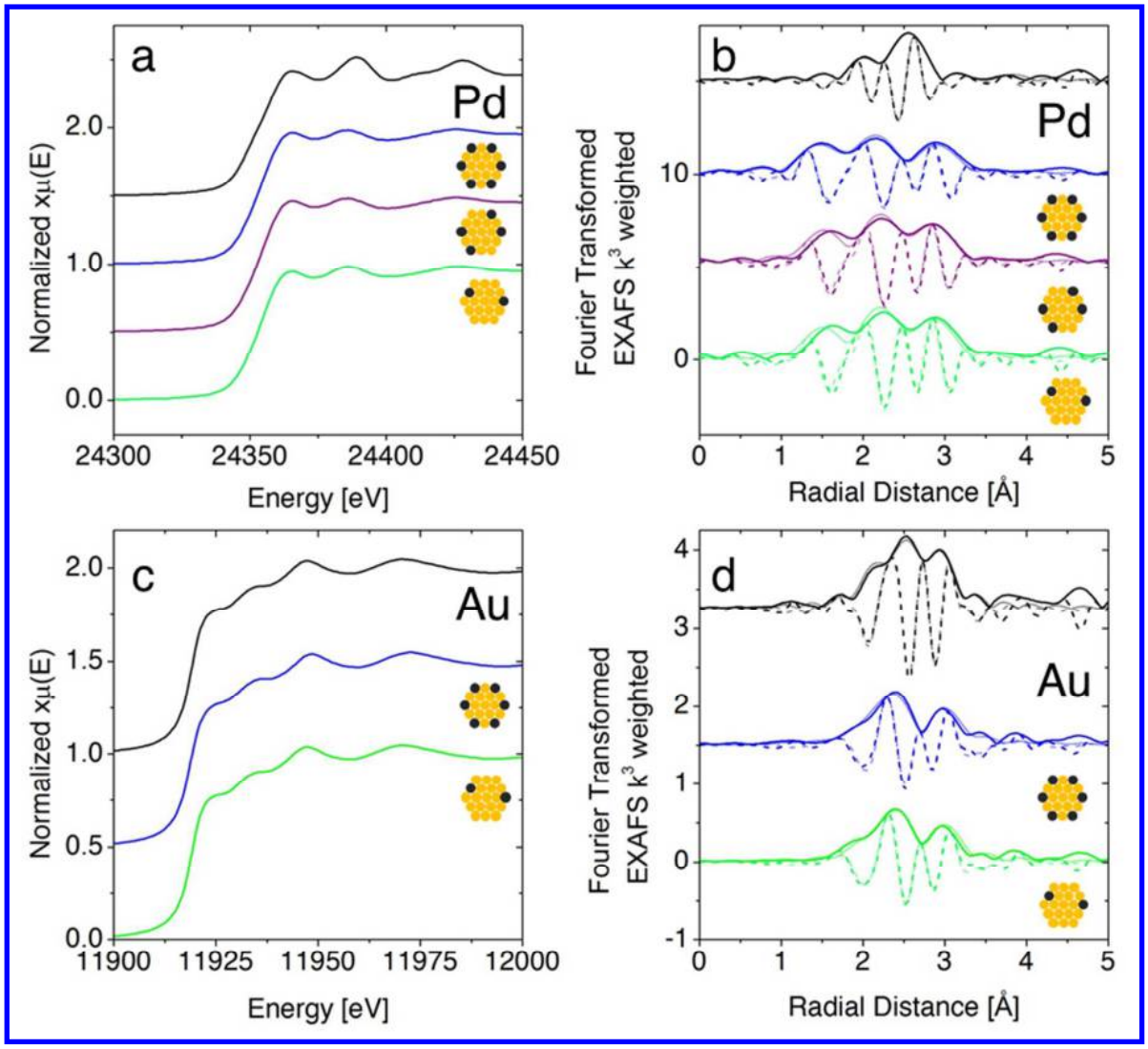


**Figure 4.** Pd-K edge and Au $L_3$-edge XANES (a and c respectively) for Pd(1.4%)/Au (green), Pd(4.1%)/Au (purple), and Pd(7.0%)/Au (blue) along with Pd or Au foils (black). Fourier-transform EXAFS at the Pd K-edge and Au-$L_3$ edge with model fits (b and d respectively) where the dark lines represents data, the faded lines represent best-fit models, solid lines represent Fourier-transform magnitude and dotted lines represent the imaginary component of the Fourier-transform.

**Table 1.** Best fit parameters from the modeling of the EXAFS data collected at the Pd-K edge and Au $L_3$-edge.

| Sample | Scattering Path | Radial Distance [Å] | Coordination Number | $\sigma^2$ [Å$^2$] | $\Delta E_0$ [eV] | R-factor [%] |
|---|---|---|---|---|---|---|
| Pd (7.0%)/Au | Pd-Pd | 2.75 ± 0.04 | 0.3 ± 0.4 | 0.0030 ± 0.0006 | -1.6 ± 0.5 | 2.1 |
| | Pd-O | 2.01 ± 0.02 | 1.4 ± 0.5 | 0.007 ± 0.006 | | |
| | Pd-Au | 2.822 ± 0.007 | 8 ± 2 | 0.012 ± 0.004 | | |
| | | | | | | |
| | Au-Au | 2.845 ± 0.009 | 10 ± 1 | 0.010 ± 0.001 | 6.5 ± 0.8 | 1.9 |
| | Au-Pd | 2.84 ± 0.03 | 0.6 ± 0.3 | 0.003 ± 0.001 | | |
| | | | | | | |
| Pd (4.1%)/Au | Pd-Pd | 2.75 ± 0.04 | 0.0 ± 0.5 | 0.0030 ± 0.0006 | -1.6 ± 0.5 | 2.1 |
| | Pd-O | 2.01 ± 0.02 | 1.4 ± 0.6 | 0.007 ± 0.006 | | |
| | Pd-Au | 2.822 ± 0.007 | 9 ± 3 | 0.012 ± 0.004 | | |
| | | | | | | |
| Pd (1.4%)/Au | Pd-Pd | 2.75 ± 0.04 | 0.0 ± 0.5 | 0.0030 ± 0.0006 | -1.6 ± 0.5 | 2.1 |
| | Pd-O | 2.01 ± 0.02 | 1.3 ± 0.6 | 0.007 ± 0.006 | | |
| | Pd-Au | 2.822 ± 0.007 | 10 ± 2 | 0.012 ± 0.004 | | |
| | | | | | | |
| | Au-Au | 2.845 ± 0.009 | 11 ± 2 | 0.010 ± 0.001 | 6.5 ± 0.8 | 1.9 |
| | Au-Pd | 2.84 ± 0.03 | 0.2 ± 0.3 | 0.003 ± 0.001 | | |

From the perspective of Pd, the smoothing out of the Pd K-edge XANES relative to those of the Pd foil indicates a low total coordination. The EXAFS spectra exhibit minor Pd-Pd coordination as well as that of both Pd-O and Pd-Au. For all samples, the Pd-Pd coordination number is close to zero within experimental error, indicating that the majority of Pd atoms in the alloy are isolated from other Pd atoms, confirming that a dilute or single-atom alloy has been formed. The data in Table S2 shows that as the fraction of Pd in the NC increased from 1.4 % to 10.5 %, the Pd-Pd coordination increased from zero to 1.1 ± 0.4 as the probability of adjacent Pd

atoms increased. The Pd-Au coordination numbers in the range of 8-10 indicate that Pd is incorporated into an alloy with Au. The Pd-Au bond length (2.82 ± 0.01 Å) is intermediate to either pure metal (2.736 ± 0.002 Å for Pd and 2.860 ± 0.003 Å for Au) and is consistent with bond lengths reported in the literature for Pd/Au alloys.[34,35] Pd is partially oxidized, as evidenced by Pd-O coordination numbers of 1.3-1.4. The Au-Pd coordination numbers of 0.2-0.6 indicate a minor content of Pd, while Au-Au coordination numbers as high as 10-11 are consistent with nanoparticles being large enough to contain the dominant fraction of atoms in the bulk. Unlike Pd, oxidation of Au was not observed.

In terms of the distribution of Pd among Au, Figure 5 shows a good match of the model for surface alloying with experimentally determined coordination numbers on all 8 analyzed samples. The Pd-Au coordination numbers were clearly below 9, indicating that Pd was located on the surface atomic layer, and decrease with increasing $x_{Pd}/D$ as predicted. The Pd-Pd coordination numbers are systematically over-estimated by the model. This is due to the fact that Pd is partly oxidized, with oxygen located in between neighboring Pd atoms that would otherwise be direct neighbors. The surface location of Pd was further supported by contrasting it with a bulk location of Au, seen by the sum of Au-Pd and Au-Au coordination numbers approaching 12 in Figure S4. Bulk alloying of Pd with Au was not supported, since the experimental coordination numbers in Figure S5 did not match the bulk alloy model.

The dilute nature of the catalysts made the application of several characterization techniques challenging. The low amount of Pd present in small nanoparticles did not provide sufficient contrast to resolve in STEM-EDS and the low total metal loading did not provide sufficient material for XRD patterns to be resolved for Au, Pd, or Pd/Au. However, The XAS,

TEM, and UV-vis analysis together demonstrate that the colloidal NCs are indeed Pd/Au alloys in the dilute or SAA regime with fine control over size, composition, and metal loading.

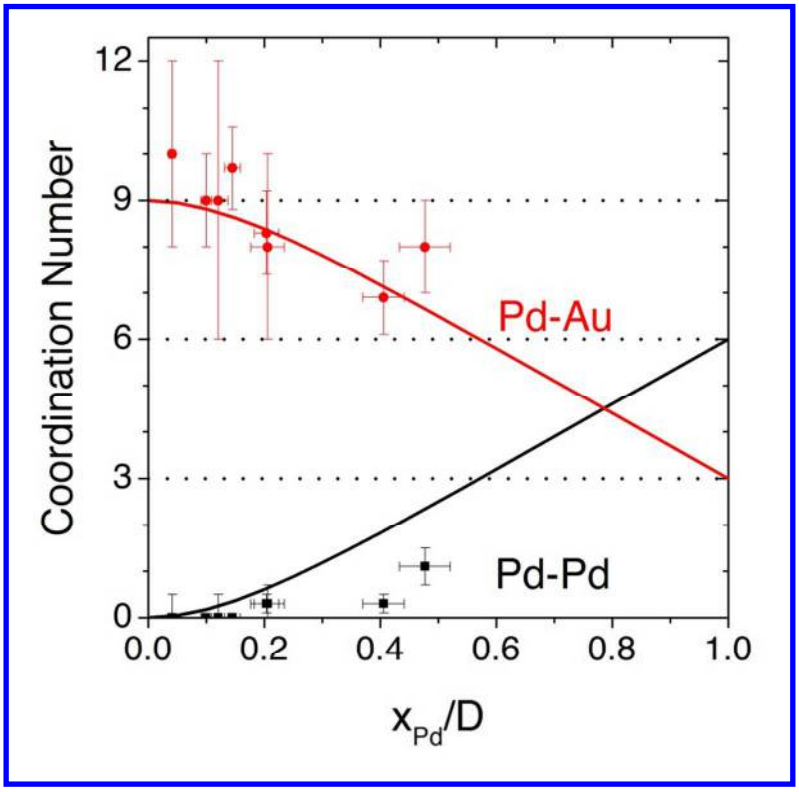


**Figure 5.** Pd-Pd and Pd-Au coordination numbers predicted by the surface-alloy model (solid lines), overlaid with experimentally determined coordination numbers from all 8 samples analyzed by XAS.

The series of three 2.8 nm Pd/Au/$TiO_2$ catalysts with low, intermediate, and high amounts of Pd, together with Au/$TiO_2$ and Pd/$TiO_2$ were tested for the selective oxidation of 2-propanol to acetone at atmospheric pressure to examine the impact of structure and composition on the Pd/Au/$TiO_2$ catalytic performance under hydro-oxidation conditions. We focused on the

small NC series of catalysts because of the known high activity of Au catalysts in the sub-5 nm size regime,[36] and because catalytic trends in activity and selectivity were similar for catalysts with larger particles (Figure S6). For these experiments, the alloy sample with intermediate Pd content was re-synthesized with similar size and Pd loadings (3.3 nm and Pd (4.8%)/Au/$TiO_2$. See Figure S7 for characterization) but the same catalyst geometry consisting of single Pd atoms dispersed in Au NCs. The presence of selective oxidizing species created by the combination of hydrogen and oxygen was probed by measuring the difference in acetone production between oxidation and hydro-oxidation conditions (see Scheme 2). This difference is particularly important for Pd containing catalysts as Pd is known to convert 2-propanol to acetone in the oxidation pathway.[37] The reactor feed contained 0.25 vol. % 2-propanol, 2.5 vol. % $O_2$, and optionally 2.5 vol. % $H_2$. Identical reaction conditions were used for all samples to allow for comparison.

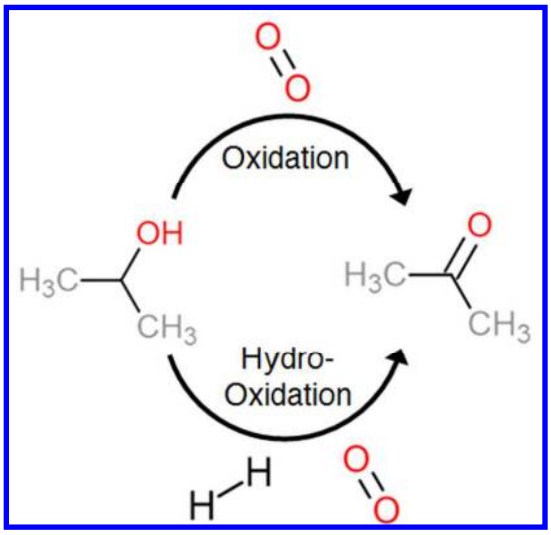


**Scheme 2.** Pathways to oxidize 2-propanol to acetone that are being examined that include only oxygen (oxidation, top path) or a combination of hydrogen and oxygen (hydro-oxidation, bottom path).

Figure 6 shows the yield of acetone (the product of selectivity to acetone and 2-propanol conversion) for $Au/TiO_2$, $Pd/Au/TiO_2$ and $Pd/TiO_2$ catalysts with and without hydrogen included in the feed stream. In the absence of co-fed hydrogen (oxidation conditions), it can be seen that $Pd/TiO_2$ is the most active catalyst for the oxidation of 2-propanol to acetone, with activity starting at 75 °C, while Au does not become active until 125 °C. The Pd/Au alloys span the difference between the two pure metals, with larger amounts of Pd leading to higher activities at lower temperatures. With respect to selectivity, the pure Pd catalyst never reaches 100% acetone yield under our experimental conditions due to the commencement of complete combustion near 100 °C, and produces only carbon dioxide by 200 °C. In the presence of co-fed hydrogen (hydro-oxidation conditions) the acetone yield for all catalysts improves to different extents. The greatest improvement is observed for the $Pd/Au/TiO_2$ catalysts where full conversion is already

approached by 100 °C in the Pd(7.0%)/Au/$TiO_2$ sample. This high activity and selectivity are maintained to temperatures greater than 200 °C. The Pd/$TiO_2$ sample improved slightly at low temperatures, reaching 100 % acetone yield at approximately 100 °C while the Au NC catalyst also showed higher activity at lower temperatures while maintaining 100% selectivity to acetone. However, the pure Au catalyst never approached 100 % conversion in the temperature regime explored here.

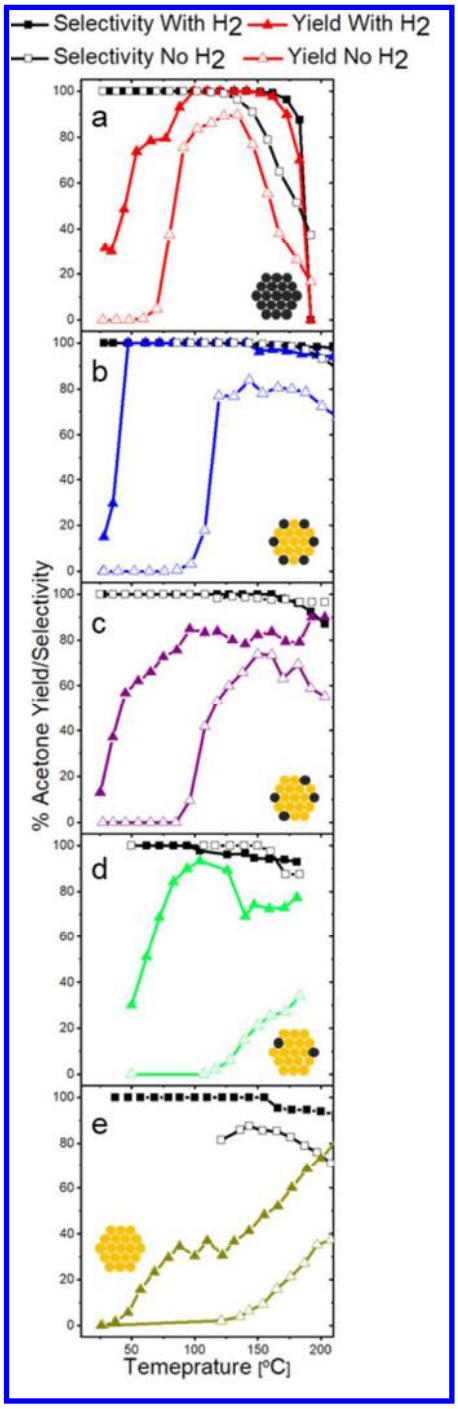


**Figure 6.** Acetone yield and selectivity as a function of temperature for (a) 2.9 nm $Pd/TiO_2$, (b) 2.8 nm $Pd(7.0\%)/Au/TiO_2$, (c) 3.3 nm $Pd(4.8\%)/Au/TiO_2$, (d) 2.8 nm $Pd(1.4\%)/Au/TiO_2$, and (e) 2.8 nm $Au/TiO_2$. Open symbols denote catalyst activity under oxidation conditions while filled

symbols denote catalyst activity under hydro-oxidation conditions. Triangles denote acetone yield while squares denote acetone selectivity.

The difference in activity between oxidation and hydro-oxidation conditions is summarized in Figure 7 where the difference in acetone yield is compared for all catalysts. The comparison is made at both 75 °C (Figure 7a) and 125 °C (Figure 7b). While the improvement for the Pd/Au alloys is less obvious at 125 °C due to higher activity of the oxidation pathway, there is a clear trend for the Pd/Au alloy catalysts at 75 °C, where the oxidation pathway is not active. The formation of hydrogen peroxide, a potential selective oxidizing species, is known to be favorable at lower temperatures because of its tendency to quickly decompose at higher temperatures.[10] For this reason, the trend at 75 $^{o}$C strongly suggests that the formation of selective oxidizing species on the Pd/Au alloy catalysts is responsible for the improved performance. Nevertheless, the Pd(1.4%)/Au/$TiO_2$ catalyst showed the greatest increase in activity at 125 °C in large part due to its lower activity under oxidizing conditions. While all Pd/Au/$TiO_2$ catalysts reached nearly 100% acetone yield under hydro-oxidation conditions at 125 °C, the Pd(7.0%)/Au/$TiO_2$ catalyst also showed high activity under oxidizing conditions, leading to a low difference in Figure 7b. This result is in agreement with the Pd(7.0%)/Au/$TiO_2$ catalyst behaving more closely to Pd, which is also very active for converting 2-propanol to acetone under oxidizing conditions. As a result, the hydro-oxidation pathway appears to be less important on the high-Pd content alloys for this reaction.

An additional consideration for comparing catalysts operating at 75 °C and 125 °C temperatures comes from long term stability tests, which showed that the catalysts deactivated

over the course of one day at 75 °C (Figure S8). Sintering is not the mechanism for catalyst deactivation as Pd/Au/$TiO_2$ maintained their particle shape under reaction conditions as confirmed by TEM (Figure 2 b-c). The deactivation is likely due to the strong binding of intermediates or byproducts at the NC/support interface similar to what is observed for propylene epoxidation catalysts.[38] Results of long-term testing at 125 °C indeed show that the samples are much more stable, likely because of weaker adsorption of intermediate species, while still providing 100% selectivity to acetone (Figure S8).

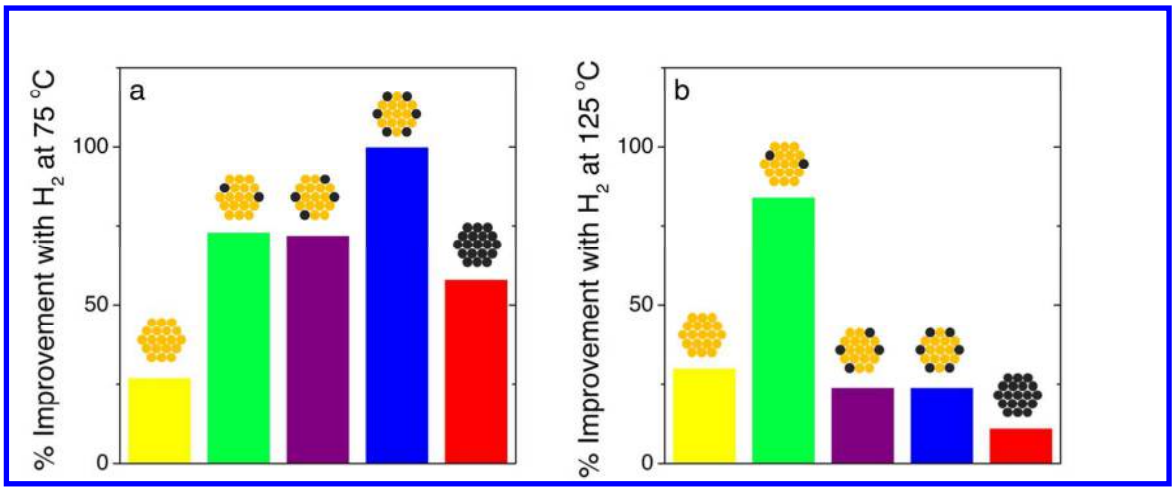


**Figure 7.** Percent improvement in acetone yield between hydro-oxidation and oxidation conditions at (a) 75 °C and (b) 125 °C for Au/$TiO_2$ (yellow), Pd (1.4%)/Au/$TiO_2$ (green), Pd(4.8%)/Au/$TiO_2$ (purple) Pd(7.0%)/Au/$TiO_2$ (blue), and Pd/$TiO_2$ (red).

While the Pd/$TiO_2$ catalyst also shows enhanced activity in the hydro-oxidation pathway at 75 °C, it shows the least improvement at 125 °C. This difference is likely a result of the ability of Pd to dissociatively chemisorb oxygen at elevated temperatures.[22,23] The breaking of the

oxygen-oxygen bond will disrupt the formation of hydroperoxy intermediates under hydro-oxidation conditions. However, $Pd/TiO_2$ maintains higher selectivity at temperatures above 150 °C under hydro-oxidation conditions than under oxidizing conditions. This increase in selectivity is likely a result of water produced under hydro-oxidation conditions which decreases the Pd combustion activity.[39]

To prove that water, which could be produced in large amounts under hydro-oxidation conditions, was not responsible for the high activity of Pd/Au catalysts, an experiment with a water co-feed replacing hydrogen was conducted using the $Pd(1.4\%)/Au/TiO_2$ catalyst at 125 °C. The level of water was selected to match the amount of water that would be produced by complete combustion of the hydrogen feed with oxygen (2.5 vol. %). Under these conditions no acetone was produced (Figure S9). However, once the water flow was stopped and replaced by a 2.5 vol. % $H_2$ feed, the conversion of 2-propanol to acetone resumed on the same catalyst bed, albeit at lower rates likely due to water adsorption on active sites. This indicates that the benefit of the hydro-oxidation conditions extend beyond simply forming water to transiently poison the activity of Pd for combustion.

To further elucidate the role of isolated Pd atom geometries in enhancing the hydro-oxidation pathway, tests were conducted with varying the hydrogen/2-propanol ratio between 0 (no hydrogen fed) and 5. The results of these tests are presented in Figure 8. In these experiments, the total flow rate and concentration of 2-propanol and oxygen in the feed stream were maintained but an increasing concentration of hydrogen was introduced. Each data set was collected using a fresh bed of catalyst to exclude the effect of any potential non-uniform deactivation between experiments. The $Pd/TiO_2$ sample activity improves slightly below 75 °C with hydrogen but at higher temperatures the addition of hydrogen has minimal impact on

acetone yield (Figure 8a). At the same time, while hydrogen does improve the acetone yield of the $Au/TiO_2$ sample at temperatures above 100 °C, the concentration of hydrogen does not have an impact on the yield improvement and the effect is rather minimal (Figure 8b). On the other hand increasing the concentration of hydrogen in the feed increases the activity the of $Pd/Au/TiO_2$ catalyst incrementally (Figure 8c). Greater hydrogen fractions in the feed led to larger rates in the hydro-oxidation pathway, corroborating a synergistic effect between Pd single atoms and Au surfaces to produce selective oxidizing intermediates to convert 2-propanol to acetone.

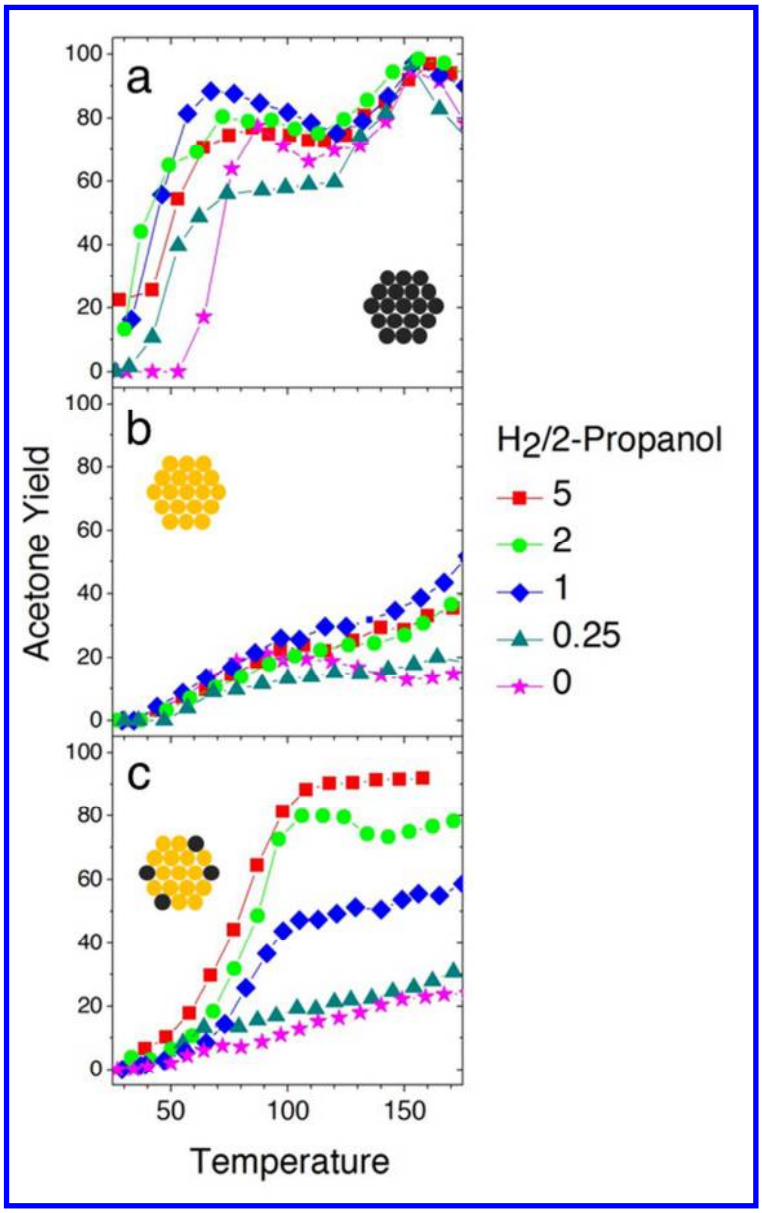


**Figure 8.** Acetone yield as a function of temperature and hydrogen/2-propanol feed ratio for (a) $Pd/TiO_2$ NC (2.8 ± 0.3 nm), (b) $Au/TiO_2$ (3.1 ± 0.4 nm), and (c) $Pd(4.8\%)/Au/TiO_2$ (3.3 ± 0.5 nm) catalysts.

The data presented in Figure 8 are summarized in Figure 9 in a metric that we label as "oxidation enhancement", which plots the difference in acetone yield between hydro-oxidation

and oxidation condition as a function of the hydrogen/2-propanol feed ratio at 150 °C. This metric shows that the Pd/Au/$TiO_2$ hydro-oxidation activity increases as a function of hydrogen addition to the feed while Au hydro-oxidation activity remains constant as a function of hydrogen above a hydrogen/2-propanol ratio of unity and Pd shows negligible hydro-oxidation activity. These findings support the proposed mechanism of hydro-oxidation where an Au-oxide interface is necessary to adsorb $O_2$ without dissociation and the inclusion of hydrogen atoms (via a hydrogen dissociation material such as Pd) enables the formation of selective oxidizing species, likely hydroperoxy intermediates. These intermediates are probably the same species hypothesized for the epoxidation of propene or for the conversion of methane to methanol.[38,40–42] Only the catalysts that contained Au showed meaningful hydro-oxidation activity coupled with high selectivity. The activity of the Pd/$TiO_2$ catalyst for the hydro-oxidation pathway may indicate that Pd is capable of this type of reaction at low temperature, where extended Pd surfaces adsorb $O_2$ but do not dissociate it. However, at higher temperatures combustion on Pd/$TiO_2$ becomes favorable, likely as Pd begins to dissociatively chemisorb $O_2$ without forming the selective oxidizing species. Single atoms of Pd in Au do not lose their hydro-oxidation activity at higher temperatures, indicating that they are not able to initiate total combustion like pure Pd. This result agrees with the high selectivity observed for all reported Pd/Au alloys. As expected, the Au catalyst hydro-oxidation activity does not improve with increasing hydrogen feeds, which supports the idea that hydrogen dissociation is the limiting step in hydro-oxidation on Au. The rate of this step is improved by adding single Pd atoms which are known to be adept at dissociating hydrogen in Pd/Au alloys.[15,18] In fact, the hydro-oxidation activity of the Pd/Au alloys improves as more hydrogen is added, indicating that the added hydrogen can be utilized to

form active oxidants and that the rate expression is dependent on hydrogen partial pressure, thus indicating that hydrogen is involved in a rate limiting step on these alloys.

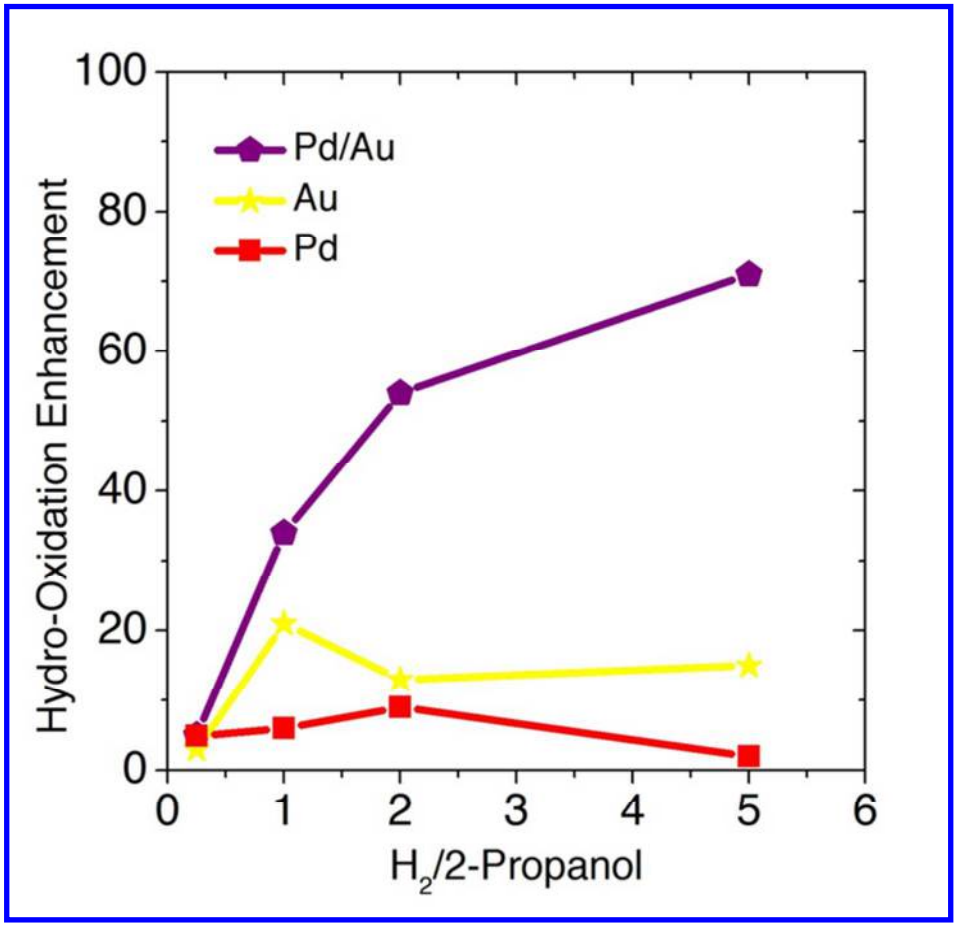


**Figure 9.** Enhancement in percent acetone yield as a function of $H_2$/2-propanol feed ratio at 150 °C.

## CONCLUSIONS

In this work we outlined a procedure to synthesize Pd/Au alloys with precisely controlled size and composition in the dilute regime, i.e. when single Pd atoms are present on the surface of Au NCs. This procedure enabled the synthesis of alloys containing single isolated atoms of Pd where the concentration of these species can be easily tuned. Alloy NC could be deposited onto metal oxide substrates while maintaining single-atom speciation of Pd. The uniformity of the catalysts and inclusion of single atoms were confirmed using TEM, UV-Vis spectroscopy, and XAS. Dilute Pd/Au alloy catalysts supported on titania were tested for the selective oxidation of 2-propanol to acetone, with particular care being given to determine their activity in the hydro-oxidation pathway which relies on selective oxidizing species produced by reaction of hydrogen and oxygen. The results show that hydro-oxidation of 2-propanol to acetone over Au catalysts is greatly improved by the inclusion of single atoms of Pd, whereas pure Pd materials are active for oxidation but catalyze combustion at high temperatures and do not show improvement under hydro-oxidation conditions. These findings support the hypothesis that hydrogen splitting is the limiting step in hydro-oxidation over Au. By alloying isolated atoms of Pd into Au even at a low concentration (1.4 at. %), hydro-oxidation activity superior to either pure metal was accomplished. This is a result of the ability of single atoms of Pd to split hydrogen while avoiding oxygen dissociation and consequent complete combustion reactions which both hinder the usefulness of Pd for selective oxidation reactions. These findings point to dilute Pd/Au alloys as a promising catalyst for future research in selective oxidation reactions through hydro-oxidation mechanisms.

## ASSOCIATED CONTENT

**Supporting Information**. The Supporting Information is available free of charge on the ACS Publications website at http://pubs.acs.org.

ICP-MS data; XAS spectra and coordination information for Pd/Au alloy NC; Additional TEM images; catalyst aging stability; catalyst activity under hydro-oxidation and wet conditions;

## AUTHOR INFORMATION

*Corresponding author: mcargnello@stanford.edu

## ACKNOWLEDGEMENT

C. J. W. acknowledges support from the Stanford Natural Gas Initiative. We gratefully acknowledge additional support from the U.S. Department of Energy, Office of Basic Energy Sciences, to the SUNCAT Center for Interface Science and Catalysis. Part of this work was performed at the Stanford Nano Shared Facilities (SNSF), supported by the National Science Foundations under award ECCS-1542152. X-ray absorption characterization experiments were performed at Beamlines 7-3 and 4-1 at the Stanford Synchrotron Radiation Lightsource (SSRL) of SLAC National Accelerator Laboratory and use of the SSRL facilities is supported by the U.S. Department of Energy, Office of Science, Office of Basic Energy Sciences under Contract No. DE-AC02-765F00515. M. C. acknowledges support from the School of Engineering at Stanford University and from a Terman Faculty Fellowship.

## REFERENCES

(1) Haruta, M.; Kobayashi, T.; Sano, H.; Yamada, N. Novel Gold Catalysts for the Oxidation of Carbon Monoxide at a Temperature Far below 0 C. *Chem. Lett.* **1987**, *16* (2), 405–408.

(2) Hayashi, T.; Tanaka, K.; Haruta, M. Selective Vapor-Phase Epoxidation of Propylene over Au / TiO 2 Catalysts in the Presence of Oxygen and Hydrogen. *J. Catal.* **1998**, *178*, 566–575.

(3) Nijhuis, T. A.; Huizinga, B. J.; Makkee, M.; Moulijn, J. A. Direct Epoxidation of Propene Using Gold Dispersed on TS-1 and Other Titanium-Containing Supports. *Ind. Eng. Chem. Res.* **1999**, *38*, 884–891.

(4) Hughes, M. D.; Xu, Y.; Jenkins, P.; Mcmorn, P.; Landon, P.; Enache, D. I.; Carley, A. F.; Attard, G. A.; Hutchings, G. J.; King, F.; Stitt E. H.; Johnston, P.; Griffin, K.; Kiely, C. J. Tunable Gold Catalysts for Selective Hydrocarbon Oxidation under Mild Conditions. *Nature* **2005**, *437* (October), 1132–1135.

(5) Saavedra, J.; Doan, H. A.; Pursell, C. J.; Grabow, L. C.; Chandler, B. D. The Critical Role of Water at the Gold-Titania Interface in Catalytic CO Oxidation. *Science (80-. ).* **2014**, *345*, 1599–1602.

(6) Mashayekhi, N. A.; Kung, M. C.; Kung, H. H. Selective Oxidation of Hydrocarbons on Supported Au Catalysts. *Catal. Today* **2014**, *238*, 74–79.

(7) Bravo-Suárez, J. J.; Bando, K. K.; Akita, T.; Fujitani, T.; Fuhrer, T. J.; Oyama, S. T. Propane Reacts with O 2 and H 2 on Gold Supported TS-1 to Form Oxygenates with High

Selectivity. *Chem. Commun.* **2008**, *28*, 3272–3274.

(8) Bravo-Suárez, J. J.; Bando, K. K.; Lu, J.; Fujitani, T.; Oyama, S. T. Oxidation of Propane to Propylene Oxide on Gold Catalysts. *J. Catal.* **2008**, *255*, 114–126.

(9) Bravo-Suárez, J. J.; Bando, K. K.; Fujitani, T.; Oyama, S. T. Mechanistic Study of Propane Selective Oxidation with H 2 and O 2 on Au / TS-1. *J. Catal.* **2008**, *257*, 32–42.

(10) Akram, A.; Freakley, S. J.; Reece, C.; Piccinini, M.; Shaw, G.; Edwards, J. K.; Desmedt, F.; Miquel, P.; Seuna, E.; Willock, D. J.; Moulijn, J. A.; Hutchings, G. J. Gas Phase Stabiliser-Free Production of Hydrogen Peroxide Using Supported Gold – Palladium Catalysts. *Chem. Sci.* **2016**, *7*, 5833–5837.

(11) Sivadinarayana, C.; Choudhary, T. V; Daemen, L. L.; Eckert, J.; Goodman, D. W. The Nature of the Surface Species Formed on Au / TiO 2 during the Reaction of H 2 and O 2 : An Inelastic Neutron Scattering Study. *J. Am. Chem. Soc.* **2004**, *126*, 38–39.

(12) Bravo-Suárez, J. J.; Bando, K. K.; Lu, J.; Haruta, M.; Fujitani, T.; Oyama, S. T. Transient Technique for Identification of True Reaction Intermediates : Hydroperoxide Species in Propylene Epoxidation on Gold / Titanosilicate Catalysts by X-Ray Absorption Fine Structure Spectroscopy. *J. Phys. Chem. C* **2008**, *112*, 1115–1123.

(13) Green, I. X.; Tang, W.; Neurock, M.; Yates Jr, J. T. Low-Temperature Catalytic H 2 Oxidation over Au Nanoparticle / TiO 2 Dual Perimeter Sites. *Angew. Chem. Int. Ed. Engl.* **2011**, *50*, 10186–10189.

(14) Naito, S.; Mitsutoshi, T. Oxygen Enhanced Hydrogen Exchange and Hydrogenation over Supported Gold Catalysts. *J. Chem. Soc. Chem. Commun.* **1988**, *12*, 832–833.

(15) Kyriakou, G.; Boucher, M. B.; Jewell, A. D.; Lewis, E. A.; Lawton, T. J.; Baber, A. E.; Tierney, H. L.; Flytzani-Stephanopoulos, M.; Sykes, E. C. H. Isolated Metal Atom Geometries as a Strategy for Selective Heterogeneous Hydrogenations. *Science (80-. ).* **2012**, *335* (March), 1209–1213.

(16) Kruppe, C. M.; Krooswyk, J. D.; Trenary, M. Selective Hydrogenation of Acetylene to Ethylene in the Presence of a Carbonaceous Surface Layer on a Pd / Cu ( 111 ) Single-Atom Alloy. *ACS Catal.* **2017**, *7*, 8042–8049.

(17) Lucci, F. R.; Marcinkowski, M. D.; Lawton, T. J.; Sykes, E. C. H. H 2 Activation and Spillover on Catalytically Relevant Pt–Cu Single Atom Alloys. *J. Phys. Chem. C* **2015**, *119* (43), 24351–24357.

(18) Lucci, F. R.; Darby, M. T.; Mattera, M. F. G.; Ivimey, C. J.; Therrien, A. J.; Michaelides, A.; Stamatakis, M.; Sykes, E. C. H. Controlling Hydrogen Activation, Spillover, and Desorption with Pd–Au Single-Atom Alloys. *J. Phys. Chem. Lett.* **2016**, *7* (3), 480–485.

(19) Aich, P.; Wei, H.; Basan, B.; Kropf, A. J.; Schweitzer, N. M.; Marshall, C. L.; Miller, J. T.; Meyer, R. Single-Atom Alloy Pd − Ag Catalyst for Selective Hydrogenation of Acrolein. *J. Phys. Chem. C* **2015**, *119*, 18140–18148.

(20) Boucher, M. B.; Zugic, B.; Cladaras, G.; Kammert, J.; Marcinkowski, M. D.; Lawton, T. J.; Sykes, E. C. H.; Flytzani-Stephanopoulos, M. Single Atom Alloy Surface Analogs in Pd0.18Cu0.15 Nanoparticles for Selective Hydrogenation Reactions. *Phys. Chem. Chem. Phys.* **2013**, *15*, 12187–12196.

(21) Liu, J.; Lucci, F. R.; Yang, M.; Lee, S.; Marcinkowski, M. D.; Therrien, A. J.; Williams,

C. T.; Sykes, E. C. H.; Flytzani-Stephanopoulos, M. Tackling CO Poisoning with Single-Atom Alloy Catalysts. *J. Am. Chem. Soc.* **2016**, *138* (20), 6396–6399.

(22) Gao, F.; Wang, Y.; Goodman, D. W. CO Oxidation over AuPd(100) from Ultrahigh Vacuum to Near-Atmospheric Pressures: The Critical Role of Contiguous Pd Atoms. *J. Am. Chem. Soc.* **2009**, *131* (16), 5734–5735.

(23) Han, S.; Mullins, C. B. Surface Alloy Composition Controlled O 2 Activation on Pd–Au Bimetallic Model Catalysts. *ACS Catal.* **2018**, *8* (4), 3641–3649.

(24) Biella, S.; Rossi, M. Gas Phase Oxidation of Alcohols to Aldehydes or Ketones Catalysed by Supported Gold. *Chem. Commun.* **2003**, *3*, 378–379.

(25) Sobolev, V. I.; Koltunov, K. Y.; Simakova, O. A.; Leino, A.; Murzin, D. Y. Low Temperature Gas-Phase Oxidation of Ethanol over Au/TiO2. *Appl. Catal. A Gen.* **2012**, *433–434*, 88–95.

(26) Abad, A.; Concepción, P.; Corma, A.; Garcia, H. A Collaborative Effect between Gold and a Support Induces the Selective Oxidation of Alcohols. *Angew. Chem. Int. Ed. Engl.* **2005**, *44*, 4066–4069.

(27) Wu, Y. Y.; Kung, H. H. Probing Properties of the Interfacial Perimeter Sites in TiO x / Au / SiO 2 with 2-Propanol Decomposition. *Appl. Catal. A, Gen.* **2017**, *548* (April), 150–163.

(28) Peng, S.; Lee, Y.; Wang, C.; Yin, H.; Dai, S.; Sun, S. A Facile Synthesis of Monodisperse Au Nanoparticles and Their Catalysis of CO Oxidation. *Nano Res.* **2008**, *1*, 229–234.

(29) Willis, J. J.; Gallo, A.; Sokaras, D.; Aljama, H.; Nowak, S. H.; Goodman, E. D.; Wu, L.; Tassone, C. J.; Jaramillo, T. F.; Abild-Pedersen, F.; Cargnello, M. Systematic Structure–

Property Relationship Studies in Palladium-Catalyzed Methane Complete Combustion. *ACS Catal.* **2017**, *7* (11), 7810–7821.

(30) Cargnello, M.; Agarwal, R.; Klein, D. R.; Diroll, B. T.; Agarwal, R.; Murray, C. B. Uniform Bimetallic Nanocrystals by High-Temperature Seed-Mediated Colloidal Synthesis and Their Catalytic Properties for Semiconducting Nanowire Growth. *Chem. Mater.* **2015**, *27* (16), 5833–5838.

(31) Cargnello, M.; Chen, C.; Diroll, B. T.; Doan-Nguyen, V. V. T.; Gorte, R. J.; Murray, C. B. Efficient Removal of Organic Ligands from Supported Nanocrystals by Fast Thermal Annealing Enables Catalytic Studies on Well-Defined Active Phases. *J. Am. Chem. Soc.* **2015**, *137*, 6906–6911.

(32) Ravel, B.; Newville, M. ATHENA, ARTEMIS, HEPHAESTUS: Data Analysis for X-Ray Absorption Spectroscopy Using IFEFFIT. *J. Synchrotron Radiat.* **2005**, *12* (4), 537–541.

(33) Spenadel, L.; Boudart, M. Dispersion of Platinum on Supported Catalysts. *J. Phys. Chem.* **1960**, *64* (2), 204–207.

(34) Fang, Y.; Miller, J. T.; Guo, N.; Heck, K. N.; Alvarez, P. J. J.; Wong, M. S. Structural Analysis of Palladium-Decorated Gold Nanoparticles as Colloidal Bimetallic Catalysts. *Catal. Today* **2011**, *160*, 96–102.

(35) Gibson, E. K.; Beale, A. M.; Catlow, C. R. A.; Chutia, A.; Gianolio, D.; Gould, A.; Kroner, A.; Mohammed, K. M. H.; Perdjon, M.; Rogers, S. M.; Wells, P. P. Restructuring of AuPd Nanoparticles Studied by a Combined XAFS/ DRIFTS Approach. *Chem. Mater.* **2015**, *27*, 3714–3720.

(36) Lee, W. S.; Zhang, R.; Akatay, M. C.; Baertsch, C. D.; Stach, E. A.; Ribeiro, F. H.; Delgass, W. N. Differences in Catalytic Sites for CO Oxidation and Propylene Epoxidation on Au Nanoparticles. *ACS Catal.* **2011**, *1* (10), 1327–1330.

(37) Groppo, E.; Lazzarini, A.; Carosso, M.; Bugaev, A.; Manzoli, M.; Pellegrini, R.; Lamberti, C.; Banerjee, D.; Longo, A. Dynamic Behavior of Pd/P4VP Catalyst during the Aerobic Oxidation of 2-Propanol: A Simultaneous SAXS/XAS/MS Operando Study. *ACS Catal.* **2018**, *8* (8), 6870–6881.

(38) Nijhuis, T. A.; Visser, T.; Weckhuysen, B. M. The Role of Gold in Gold–Titania Epoxidation Catalysts. **2005**, 1115–1118.

(39) Ciuparu, D.; Pfefferle, L. Support and Water Effects on Palladium Based Methane Combustion Catalysts. *Appl. Catal. A Gen.* **2001**, *209* (1–2), 415–428.

(40) Nijhuis, T. A.; Visser, T.; Weckhuysen, B. M. Mechanistic Study into the Direct Epoxidation of Propene over Gold/Titania Catalysts. *J. Phys. Chem. B* **2005**, *109* (41), 19309–19319.

(41) Nijhuis, T. A.; Sacaliuc-Parvulescu, E.; Govender, N. S.; Schouten, J. C.; Weckhuysen, B. M. The Role of Support Oxygen in the Epoxidation of Propene over Gold-Titania Catalysts Investigated by Isotopic Transient Kinetics. *J. Catal.* **2009**, *265* (2), 161–169.

(42) Ab Rahim, M. H.; Forde, M. M.; Jenkins, R. L.; Hammond, C.; He, Q.; Dimitratos, N.; Lopez-Sanchez, J. A.; Carley, A. F.; Taylor, S. H.; Willock, D. J.; Murphy, D. M.; Kiely, C. J.; Hutchings, G. J. Oxidation of Methane to Methanol with Hydrogen Peroxide Using Supported Gold-Palladium Alloy Nanoparticles. *Angew. Chem. Int. Ed.* **2013**, *52* (4),

1280–1284.

**TOC Graphic**

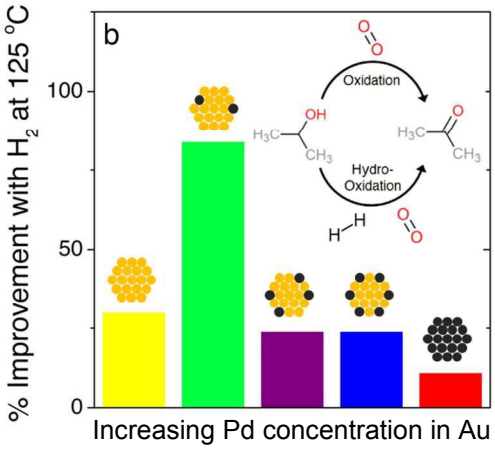
b
% Improvement with $H_2$ at 125 °C
100
50
0
Oxidation
Hydro-
Oxidation
Increasing Pd concentration in Au